www.sciencemag.org/content/363/6434/eaat9691/suppl/DC1

Supplementary Materials for

Bacteriophage trigger antiviral immunity and prevent clearance of bacterial infection

Johanna M. Sweere, Jonas D. Van Belleghem, Heather Ishak, Michelle S. Bach, Medeea Popescu, Vivekananda Sunkari, Gernot Kaber, Robert Manasherob, Gina A. Suh, Xiou Cao, Christiaan R. de Vries, Dung N. Lam, Payton L. Marshall, Maria Birukova, Ethan Katznelson, Daniel V. Lazzareschi, Swathi Balaji, Sundeep G. Keswani, Thomas R. Hawn, Patrick R. Secor, Paul L. Bollyky*

*Corresponding author. Email: pbollyky@stanford.edu

Published 29 March 2019, *Science* **363**, eaat9691 (2019)
DOI: 10.1126/science.aat9691

This PDF file includes:

Other Supplementary Materials for this manuscript include the following:
(available at www.sciencemag.org/content/363/6434/eaat9691/suppl/DC1)

Supplemental Materials and Methods

Phage purification

Bacteria were infected with stocks of phage at mid-log phase and cultured in 75 mL of LB broth for 48 hours at 37°C under shaking conditions. Bacteria were removed by centrifugation at 6,000 × *g* for 5 minutes, and supernatant was treated with 1 µg/mL of DNase I (Roche, Cat. No. 4716728001) for 2 hours at 37°C before sterilization by vacuum filtration through a 0.22 µm filter. In some experiments, supernatant was treated with 250 µg/mL of RNAse A (Thermo Fisher Scientifc, Cat. No. EN0531) or 85 U/mL of benzonase (Novagen, Cat No. 70746) for 4 hours at 37ºC before sterilization. Pf phage were precipitated from the supernatant by adding 0.5 M NaCl and 4% polyethylene glycol (PEG) 8000 (Milipore Sigma, Cat. No. P2139), whereas *E. coli* Fd1 phage was precipitated by 0.5 M NaCl and 4% PEG 6000 (Milipore Sigma, Cat. No. 81260). All phage solutions were incubated overnight at 4°C. Phage were pelleted by centrifugation at 13,000 × *g* for 20 minutes, and the pellet was suspended in sterile TE buffer (pH 8.0). The suspension was centrifuged for 15,000 × *g* for 20 minutes, and the supernatant was subjected to another round of PEG precipitation. The purified phage pellets were suspended in sterile PBS and dialyzed in 10-kDa molecular weight cut-off tubing (FisherScientific, Cat. No. 88243) against PBS, quantified by qPCR, diluted at least 10,000× to appropriate concentrations in sterile PBS and filter-sterilized. We sent three different Pf4 preparations diluted in PBS to working concentrations (1×10^8 Pf4/mL) to Nelson Labs (Salt Lake City, UT), where they were tested for endotoxin by *Limulus* amoebocyte lysate testing. All three preps had endotoxin levels under the test sensitivity level of 0.05 EU/mL. Phages were purified by PEG precipitation only unless noted otherwise.

Quantification of Pf phage

To quantitate Pf prophage in human or mouse wound homogenates and purified Pf phage preparations, bacterial cells and debris were removed by centrifugation at 8,000 × g for 10 min. Supernatants were boiled at 100°C for 20 min to denature any phage particles, releasing intact Pf phage DNA. 2 µL were used as a template in 20-µL qPCR reactions containing 1× SensiFAST™ Probe Hi-ROX (Bioline, Cat. No. BIO-82020), 200 nM probe, and 2 nM forward and reverse primers. For human wound swabs and Pf1 phage purifications, the primers and probe were designed to recognize PAO717, a gene conserved across the Pf phage family; for human swabs, the Pa 50S ribosomal gene rpIU was also used to confirm Pa infection. For mouse wound isolates and Pf4 phage purifications, the primers and probe were designed to recognize a Pf4 phage-specific intergenic region between PAO728 and PAO729. For the Pf phage purification preparations, levels of Pa 50S ribosomal gene rpIU were measured to correct for contaminating genomic Pa DNA, but those levels were negligible. See Table S2 for the primer and probe sequences. Cycling conditions were as follows: 95°C for 2 min, (95°C for 15 sec., 60°C for 20 sec.) × 40 cycles on a StepOnePlus Real-Time PCR system (Applied Biosystems). For the standard curve, the sequence targeted by the primers and probe were inserted into a pUC57 plasmid (Genewiz) and tenfold serial dilutions of the plasmid were used in the qPCR reactions.

In vivo murine full-thickness wound infection model

Ten-to-twelve-week old male mice were anesthetized using 3% isoflurane, and their backs were shaved using a hair clipper and further depilated using hair removal cream (Nair). The shaved area was cleaned with sterile water and disinfected twice with Betadine (Purdue Fredick Company, Cat. No. 19-065534) and 70% ethanol. Mice received 0.1-0.5 mg/kg slow-release buprenorphine (Zoopharm Pharmacy) as an analgesic. Mice received two dorsal wounds by using 6-mm biopsy punches to outline the wound area, and the epidermal and dermal layer were excised using scissors. The wound area was washed with saline and covered with Tegaderm (3M,

Cat. No. 1642W). Luminescent bacteria were grown as described above and diluted to the standard dose of $7.5 \pm 2.5 \times 10^2$ CFU/mL CFU/mL or 1×10^7 CFU/mL in PBS. Mice were inoculated with 40 µL per wound 24 hours post-wounding, and control mice were inoculated with sterile PBS. In the TNF rescue experiments, wound beds received 100 ng/wound of carrier-free TNF (Affymetrix, Cat. No. 34-8321-63) or PBS 2 hours post-inoculation. In some experiments, mice received a dose of 1×10^7 CFU/mL heat-killed bacteria, prepared as described above. Mice were weighed and imaged for luminescent signal on the IVIS Spectrum (Perkin Elmer), the Ami HTX (Spectral Instruments Imaging), or the Lago-X (Spectral Instruments Imaging) at the Stanford Center for Innovation in In Vivo Imaging daily before takedown. Uninfected mice were photographed for luminescent background correction Images were subsequently analyzed using Living Image Software (Perkin Elmer), AMIView Software (Spectral Instruments Imaging) or Aura software (Spectral Instruments Imaging). Upon takedown, wound beds were excised, minced and collected in PBS. After shaking incubation for 2 hours at 4°C, bacterial effluent was serially diluted and plated on LB agar to enumerate bacterial burden. Wounds were considered infected if luminescent signal in the wound was above background luminescence, and bacteria were detected in the wound effluent. For immune cell infiltrate analysis, wounds were processed as described in the organ immunophenotyping section in the main manuscript.

Preparation of pure phage ssDNA and amplification of individual phage genes

In order to prepare pure phage RNA, ssDNA from Pf1 (used because of higher purification yield) was extracted using the phenol chloroform method. Briefly, 500 µL of phage preparation was added to 250 µL of phenol:chloroform (Thermo Scientific, Cat. No. 17909) and vortexed twice for 30 seconds. Subsequently, the solution was centrifuged for 1 min at 12,000 × *g*. The aqueous phase was transferred to a new tube and two volumes of 25:1 ethanol:3M sodium acetate (pH 5.2) (Sigma, Cat. No. S3272-2506) were added. The solution was incubated at room temperature for 15 minutes. Following incubation, the sample was centrifuged for 10 minutes at 12,000 × *g*, after which the supernatant was removed, and the pellet was resuspended in 500 µL of 70% ethanol. The sample was centrifuged for an additional 10 minutes at 12,000 × *g*, followed by air-drying the pellet for at least 10 minutes at room temperature. Finally, the pellet was resuspended in 30 µL of TE buffer (pH 8.0) and the concentration of DNA was measured by nanodrop.

Individual phage genes were amplified using specific primers (1 µM), to which a T7 promotor was added on the forward primer, using Econotaq (Lucigen, Cat no. 30035-1). See Table S2 for the primer sequences. The PCR products were purified prior to RNA conversion. Briefly, 450 µL of 6M Guanidine Thiocyanate was added to 250 µL of PCR products and 50 µL of 3M Sodium acetate (pH 5). This mixture was added to a silicon column (Econospin, Epoch Life Sciences, Cat no. 1920-050/250,) and centrifuged for 1 minute at 12,000 × *g*. Flow-through was discarded and column was washed with 500 µL of 3M Guanidine thiocyanate and centrifuged at 12,000 × *g* for 1 minute. The column was subsequently washed by adding 500 µL of 80% ethanol and spun at 12,000 × g for 1 minute. An additional 1-minute spin at 12,000 × *g* was performed to remove any remaining trace amounts. The PCR products were eluted from the column by addition of 30 µL of nuclease-free water and centrifuged for 1 minute at 12,000 × *g*. They were subsequently converted to RNA as described in the main manuscript.

Immunofluorescent and confocal microscopy

For microscopy analysis, cells were washed three times with PBS and subsequently fixed with 10% neutral buffered formalin for 5 minutes at room temperature. After permeabilization with 0.5% Triton X-100, coverslips were washed twice with PBS and excess formalin was quenched by incubation with 150 mM glycin, pH 8.0 (Fisher BioReagents, Cat. No. BP381) for 30 minutes. Coverslips were blocked with Sea Block blocking buffer (Thermo Scientific, Cat. No. 37527) followed by incubation with primary antibodies in Sea Block overnight at 4°C. Coverslips were washed three times with PBS and incubated with the appropriate fluorescently

labeled secondary antibodies. In some experiments, phalloidin (Invitrogen, Cat. No. A12381) was added together with the secondary antibodies to visualize F-actin. All antibodies were added at the concentrations indicated in Table S3. Coverslips were mounted in ProLong Diamond Antifade Mountant (Invitrogen, Cat. No. P36970) with DAPI to label nuclei. Fluorescent specimens were examined using either conventional fluorescence microscopy (Leica DMI 6000B) or a confocal system (DMX BLAZE 3D SIM, GE Healthcare). Images were acquired using Leica DFC365 FX camera and the Leica Application Suite X (Leica). Image analysis was performed using FIJI (NIH). Movie S1 was created by capturing 0.2-µm slices with a 100× Plan Apo 1.4 NA objective (Nikon). The system used was a Nikon Ti-E chassis with a Yokugawa CSU-X1 spinning disc confocal, 405-, 488-, and 561-nm lasers, a motorized *z*-axis piezoelectric stage (Applied Scientific), and an XR/MEGA-10EX camera (Stanford Photonics) running Micro-Manger software. To create a movie out of the *z*-stack images, Imaris software (Bitplane) was used. Surface rendering was performed using the "Surfaces" feature.

Anti-CoaB mAb hybridoma cultures

After thawing, each hybridoma cell line was initially grown in DMEM media containing 10% FBS, 2 mM L-glutamine (Sigma, Cat. No. G3126), 100 IU/mL penicillin, 0.1 mg/mL streptomycin with 0.24 µg/mL amphotericin B (all from Sigma, Cat. No. A5955) and 50 mg/mL gentamicin. The clones were adapted to grow in the presence of decreasing concentrations of FBS (5%, 2.5%, 1%), while expanding from 25 cm^2 flasks to 75-175 cm^2 flasks. During the adaptation phase, the cells were cultured at 37°C in a 90% humidified atmosphere with 5% CO_2 and were maintained at the same concentration of serum for at least two passages. At the end of the adaptation phase, all lines were grown in serum-free EX-CELL Hybridoma Medium (Sigma, Cat. No. H4281).

Fig. S1

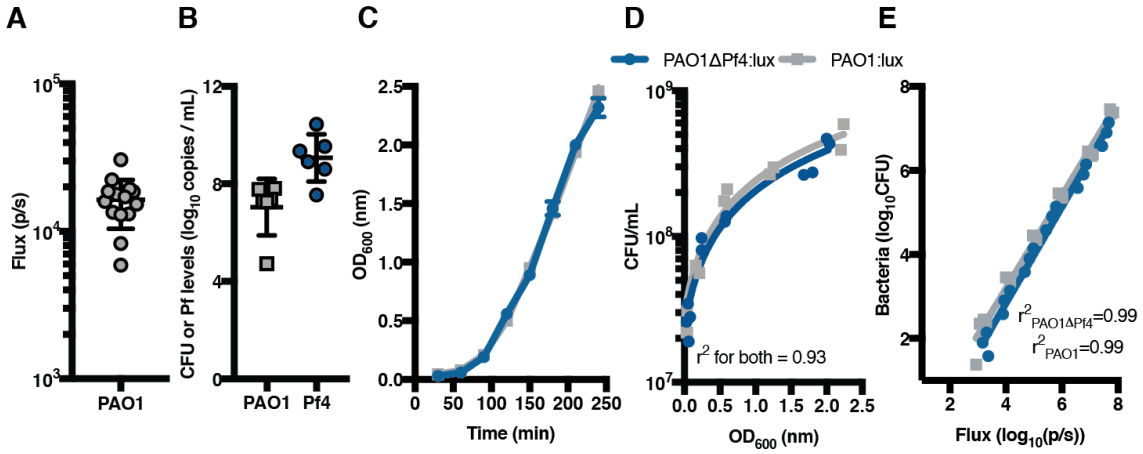

Figure S1: Full thickness wound infection model using luminescent *Pa*. A) Luminescent signal from PAO1 detected in vivo after wound inoculation with 7.5 ± 2.5 × 10^2 CFU/mL. *n*=14. B) Pf4 copy number and PAO1 CFU/mL from mouse wounds infected with planktonic PAO1, 3 days post-inoculation. C) In vitro growth rate of PAO1:lux and PAO1ΔPf4:lux strains. D) In vitro bacterial CFU correlated to OD_{600} of the PAO1:lux and PAO1ΔPf4:lux strains by linear regression analysis. Slopes were not statistically different. E) In vitro luminescence correlated to CFU of the PAO1:lux and PAO1ΔPf4:lux strains by linear regression analysis. Slopes were not statistically different. All graphs are representative of *n*=3 experiments and *n* ≥2 replicates.

Fig. S2

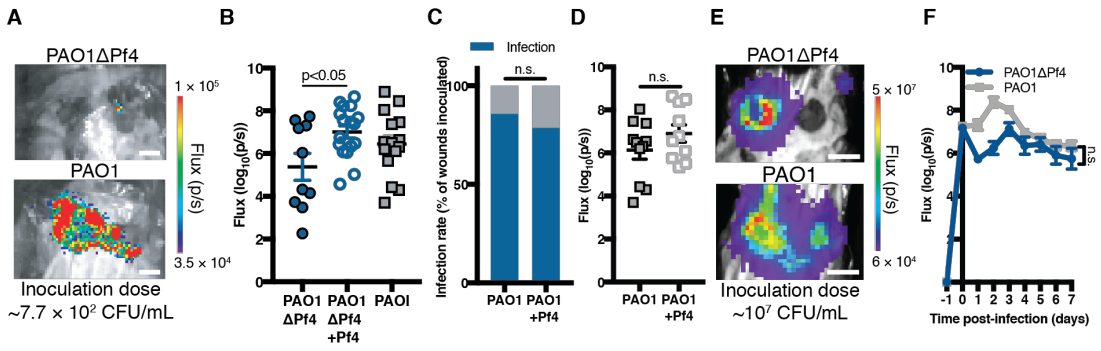

Figure S2. Pf phage exacerbates morbidity and mortality during murine full-thickness wound infection of PAO1. A) Luminescent signal from wounds infected for 3 days with 7.5 ± 2.5 × 10^2 CFU/mL of luminescent PAO1ΔPf4 or PAO1. Scale bars: 5 mm. B) Bacterial burden of wounds in experiment (Fig. 1J). Depicted are mean, SEM, analysis by one-way ANOVA with Tukey's multiple comparison. C) Infection rate in dorsal full-thickness wounds infected for 3 days with 7.5 ± 2.5 × 10^2 CFU/mL PAO1 or PAO1 supplemented with Pf4 before infection. Summary of *n*=2 experiments, *n*=12-14 wounds per group. Statistics: Fisher's exact test. D) Luminescent signal reflecting bacterial burden per wound in the experiment in (C). Depicted are mean and SEM, statistics are Student's *t*-test. E) Luminescent signal from wounds infected for 3 days with 10^7 CFU/mL luminescent PAO1ΔPf4 or PAO1. Scale bar: 5 mm. F) Bacterial burden in wounds infected with 10^7 CFU/mL PAO1ΔPf4 or PAO1. *n*=30 wounds/group, representative of *n*≥2 experiments. Depicted are mean and SEM, analysis by two-way ANOVA.

Fig. S3

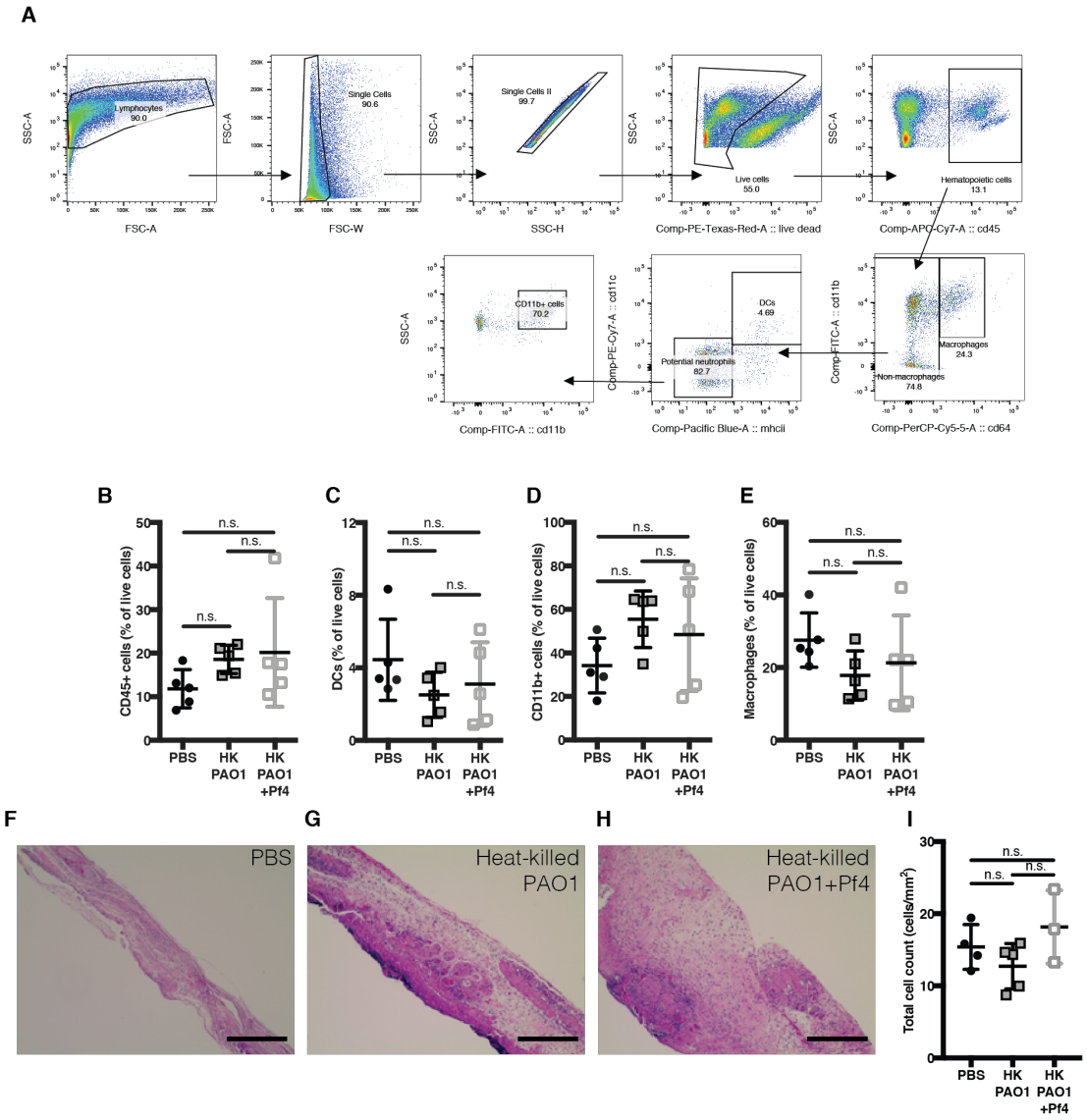

Figure S3. Analysis of inoculated wound beds for immune cell infiltrates. To accommodate for Pf4 effects on PAO1 and the different infection rates of PAO1 and PAO1ΔPf4, we performed wound inoculation experiments with heat-killed (HK) PAO1. A) Representative gating scheme for the flow cytometric analysis of wound immune infiltrates. B-E) Flow cytometric analysis of immune infiltrates of B) $CD45^+$ cells; C) dendritic cells; D) $CD11b^+$ cells, E) macrophages in wounds inoculated with PBS, HK PAO1 and HK PAO1+Pf4. Immune cells were isolated 3 days post-infection through enzymatic digestion. F-H) Representative images of hematoxylin and eosin (H&E) wound staining 3 days post-inoculation with F) PBS, G) HK PAO1 and H) HK PAO1+Pf4. Analysis of I) total wound cell count. Scale bars: 250 μm. (B-E; I) depict mean and SD. Analysis: (B-E; I) one-way ANOVA with Tukey's multiple comparison. All experiments are representative of n=3 experiments.

Fig. S4

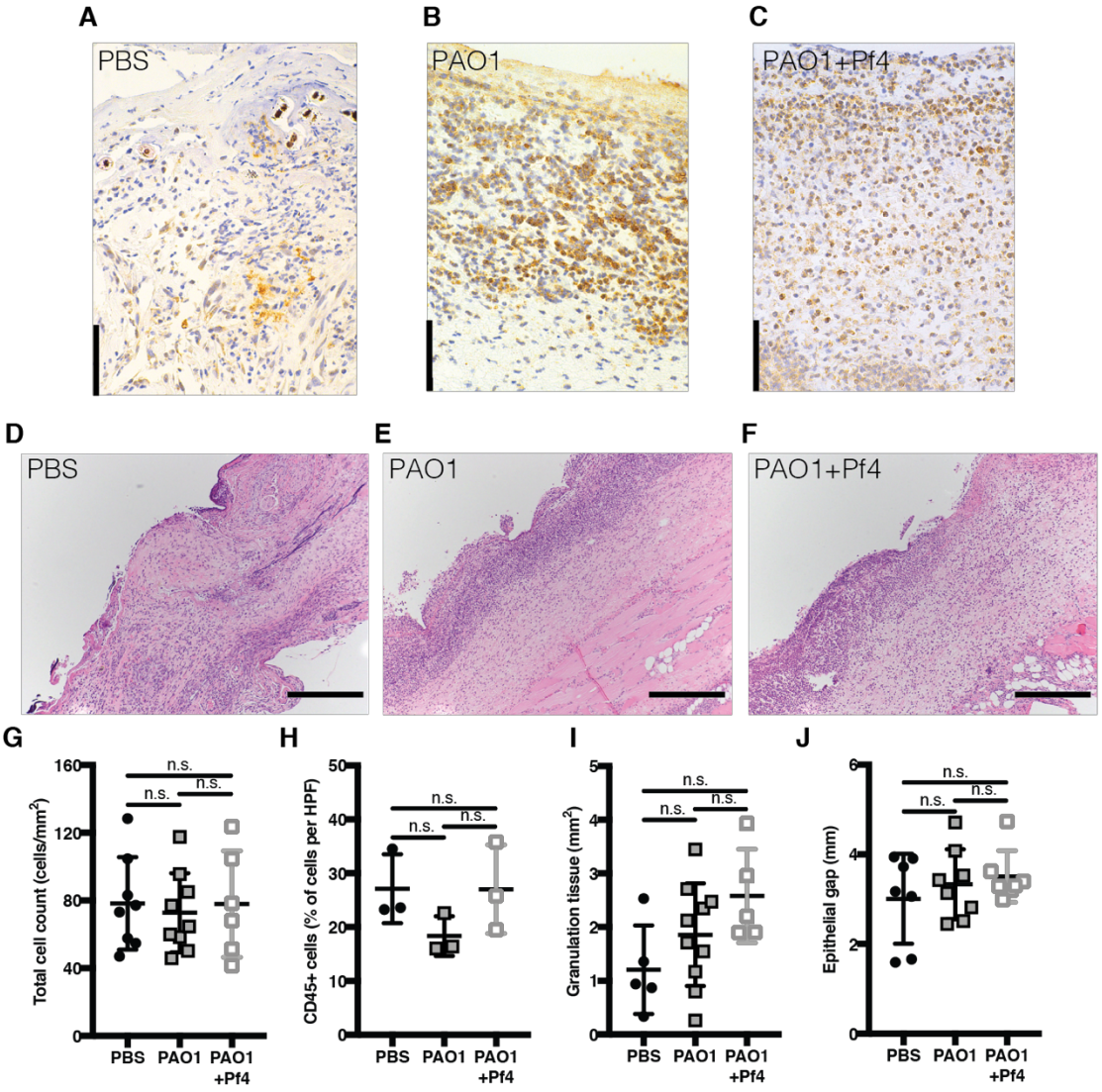

Figure S4. Analysis of inoculated wound beds for wound healing. A-C) Representative CD45 staining of wounds 3 days post-inoculation with A) PBS, B) PAO1 and C) PAO1+Pf4. Scale bars: 50 μm. D-F) Representative images of hematoxylin and eosin (H&E) wound staining 3 days post-inoculation with D) PBS, E) PAO1 and F) PAO1+Pf4. Scale bars: 250 μm. G-J) Analysis of G) total cell count; H) $CD45^+$ cells; I) granulation tissue and J) epithelial gap. (G-J) depict mean and SD. Analysis: (G-J) one-way ANOVA with Tukey's multiple comparison. All experiments are representative of n=3 experiments.

Fig. S5

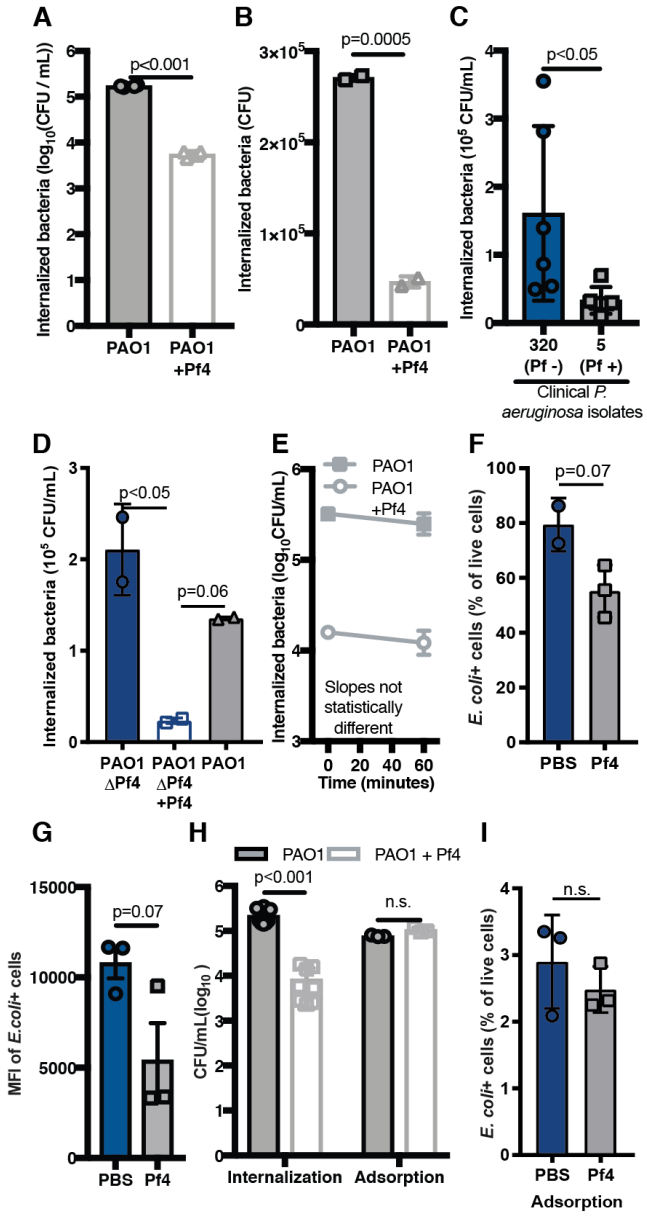

Figure S5. Pf phages inhibit phagocytosis in macrophages, but do not affect bacterial adsorption. A-B) Phagocytosis of live PAO1 and PAO1 supplemented with exogenous Pf4 (PAO1+Pf4) by A) BMDMs and B) human primary macrophages. C) Phagocytosis of human clinical *Pa* wound isolates negative (320) or positive (5) for Pf phage by BMDCs. D) Phagocytosis of live PAO1ΔPf4, PAO1ΔPf4 supplemented with exogenous Pf4 (PAO1ΔPf4+Pf4) and PAO1 by human primary macrophages. E) Linear regression analysis of intracellular killing of PAO1 or PAO1+Pf4 in BMDMs. F) Phagocytosis by BMDMs of *E. coli*-pHrodo particles in the absence or presence of purified Pf4. G) MFI of *E. coli*-pHrodo-positive cells from (F). H) BMDM cell-internalized and cell-associated PAO1 or PAO1+Pf4. I) Cell-associated *E. coli*-pHrodo in Pf4-stimulated BMDCs. (A-I) are representative of $n \geq 3$ experiments and depict mean

with SEM of $n \geq 3$ replicates; analysis: two-tailed Student's t-test. B; D) represent one blood donor and $n=2$ replicates.

Fig. S6

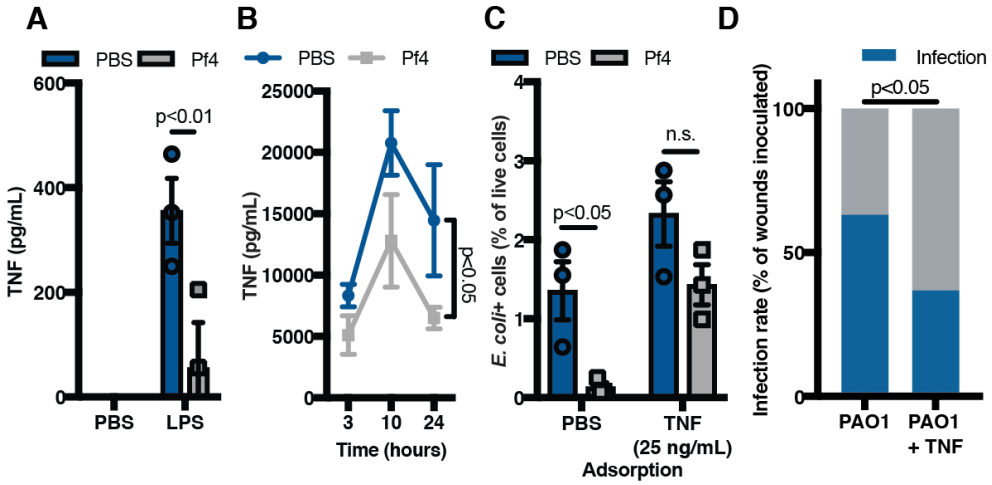

Figure S6. Pf phages inhibit phagocytosis in a TNF-dependent manner. A) TNF production in BMDMs stimulated with purified Pf4 and LPS. B) TNF production in alginate-stimulated BMDCs in response to Pf4. Time-course analysis by two-way ANOVA. C) Cell-associated *E. coli*-pHrodo in Pf4-stimulated BMDCs with exogenous TNF. (A-C) are representative of $n \geq 3$ experiments and depict mean with SEM of $n \geq 3$ replicates; analysis: (A, C) two-tailed Student's *t*-test. D) Wound infection rate 3 days post-inoculation with $7.5 \pm 2.5 \times 10^2$ CFU/mL PAO1 after treatment with PBS or TNF. Summary of $n=2$ experiments with $n=38$ wounds/group; analysis = two-tailed Fisher's exact test.

Fig. S7

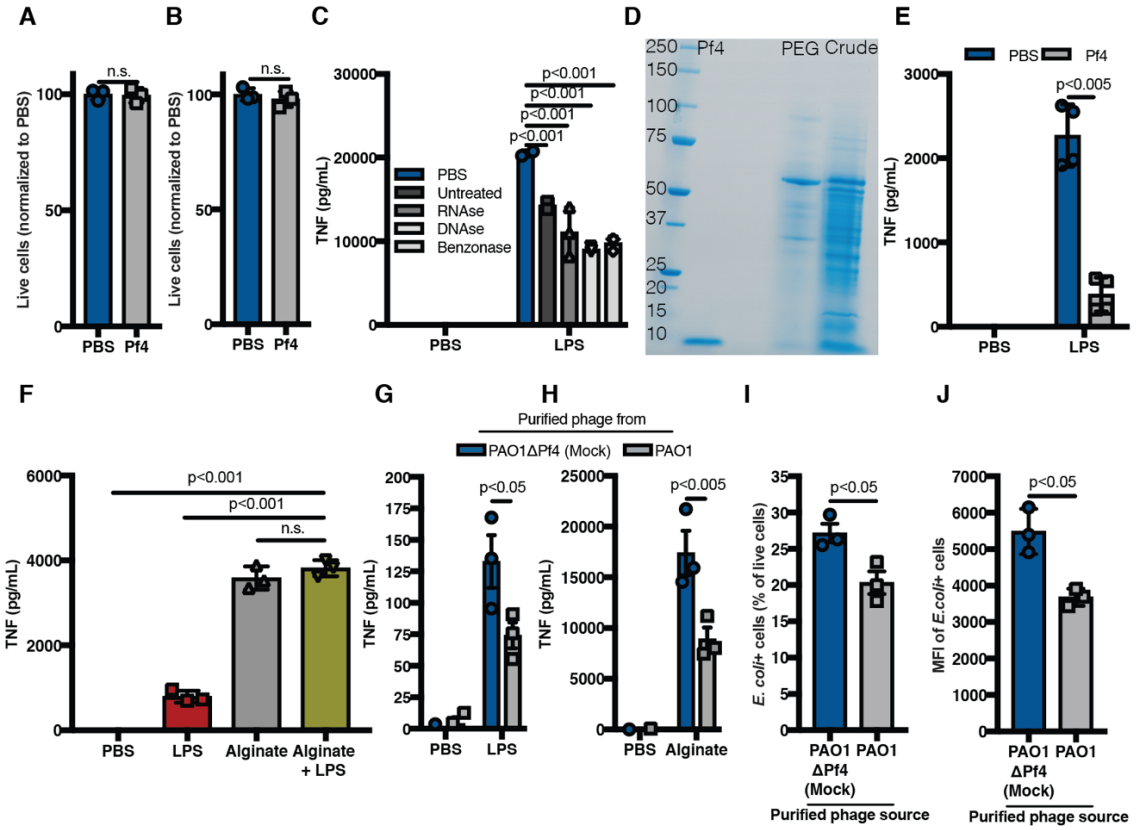

Figure S7. Pf phage-mediated immune inhibition is not due to contaminants. A-B) Live BMDCs after stimulation with A) *E. coli*-pHrodo and Pf4; B) Pf4 only. Results in (A-B) normalized to live cells in PBS condition. C) TNF production in BMDCs after 24-hour stimulation with LPS and Pf4 treated with RNAse, DNAse, benzonase or PBS. D) SDS-PAGE with purified Pf4 from the PEG-precipitation pellet (left), supernatants from PEG precipitation (middle) or crude bacterial culture (right). Band represents CoaB protein (8.4 kDa). E) TNF production in BMDCs after 24-hour stimulation with alginate and Pf4 purified by CsCl centrifugation. F) TNF production in BMDCs after 24-hour stimulation with LPS, alginate or alginate with LPS. G-J) Experiments using purified Pf4 from PAO1 or an equivalent dilution from a mock phage preparation of PAO1ΔPf4. G) TNF production in LPS-stimulated BMDCs after 24 hours. H) TNF production in alginate-stimulated BMDCs after 24 hours. I) *E. coli*-pHrodo-positive BMDCs after phage stimulation. J) MFI of *E. coli*-pHrodo-positive BMDCs treated as described in (I). All graphs are representative of $n \geq 3$ experiments and depict mean with SEM of $n \geq 3$ replicates. Statistics: two-tailed Student's *t*-test in (A, B, E, G-J); One-way ANOVA with Dunnett's multiple comparison in (C, F).

Fig. S8

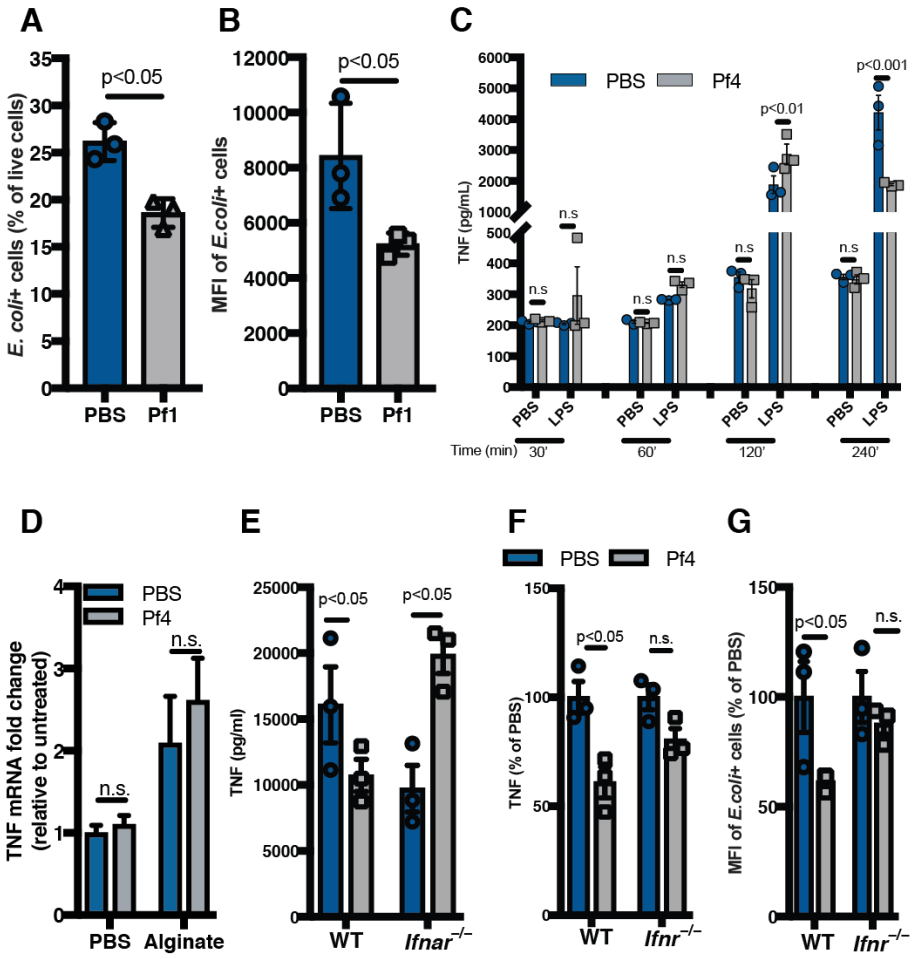

Figure S8. Pf phages inhibit TNF protein in a type I interferon-dependent manner. A) Phagocytosis by BMDCs of *E. coli*-pHrodo particles in the absence or presence of purified Pf1. B) MFI of *E. coli*-pHrodo-positive BMDCs stimulated with Pf1 phage. C) TNF production by cells used for mRNA in Fig. 3E. D) TNF mRNA upregulation in BMDCs stimulated with alginate and Pf4 for 24 hours. E) TNF production by WT or *Ifnar*$^{-/-}$ BMDCs stimulated with LPS and Pf4 phage, as shown in Fig. 3H. F) TNF production by WT or *Ifnar*/*Ifngr*$^{-/-}$ (*Ifnr*$^{-/-}$) BMDCs stimulated with alginate or Pf4 phage for 72 hours. G) MFI of *E. coli*-pHrodo particles by WT or *Ifnar*/*Ifngr*$^{-/-}$ (*Ifnr*$^{-/-}$) BMDCs stimulated with alginate and Pf4. Panels A-G) are each representative of $n \geq 3$ experiments and depict mean with SEM of $n \geq 3$ replicates. Statistics: two-tailed Student's *t*-test.

Fig. S9

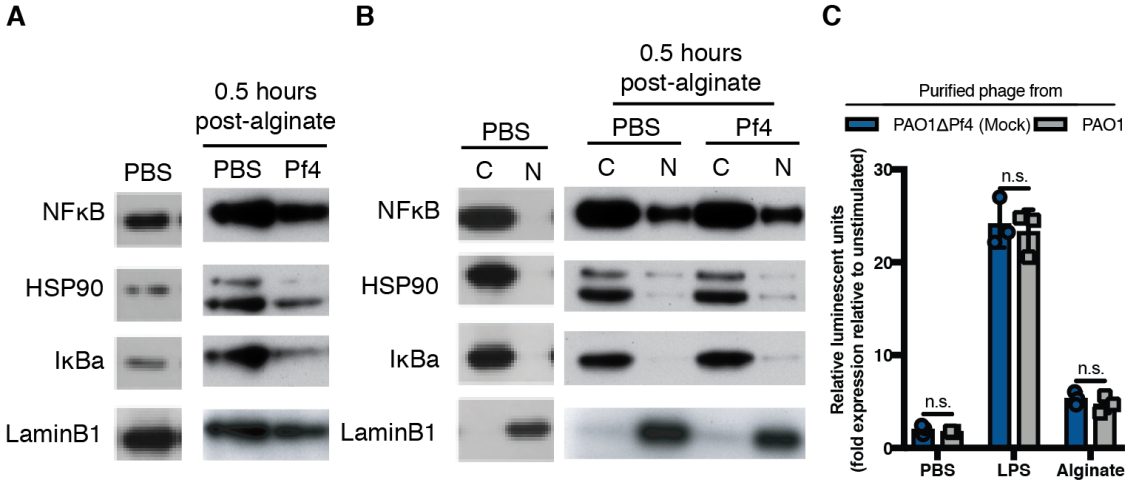

Figure S9. Pf4 does not suppress NF-κB signaling. A) Whole cell lysate of BMDCs stimulated with PBS, alginate or alginate and Pf4 for 30 minutes. B) Nuclear (N) and cytosolic (C) extracts of BMDCs stimulated with PBS, alginate or alginate and Pf4 for 30 minutes. LaminB1 was used as a nuclear marker. C) NF-κB luciferase reporter signal in RAW64.7 macrophages stimulated with LPS or alginate and Pf4 for 9 hours. The assay shown is representative of $n \geq 3$ experiments and depicts mean with SEM of $n \geq 3$ replicates. Statistics: two-tailed Student's *t*-test.

Fig. S10

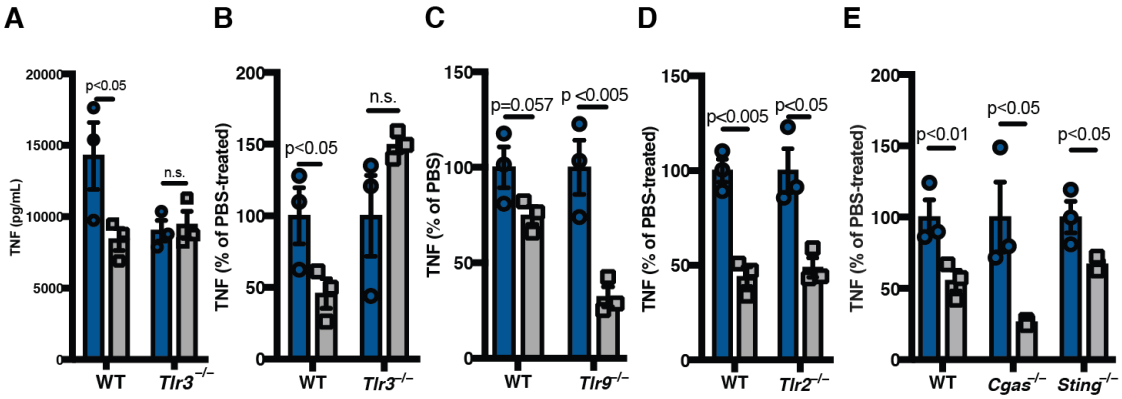

Figure S10. Pf4 phage stimulate TLR3, but not other antibacterial PRRs. A) TNF production by WT and *Tlr3*$^{-/-}$ BMDCs stimulated with alginate and Pf4, as seen in Fig. 4D. B) TNF production by WT and *Tlr3*$^{-/-}$ BMDMs stimulated with LPS and Pf4 for 24 hours. C) TNF production by WT and *Tlr9*$^{-/-}$ BMDCs stimulated with alginate and Pf4 for 24 hours. D) TNF production by WT and *Tlr2*$^{-/-}$ BMDCs stimulated with alginate and Pf4 for 48 hours. E) TNF production by WT, *Cgas*$^{-/-}$ and *Sting*$^{-/-}$ BMDCs stimulated with LPS and Pf4 for 24 hours. All graphs are representative of $n \geq 3$ experiments and depict mean with SEM of $n \geq 3$ replicates. Statistics: two-tailed Student's *t*-test.

Fig. S11

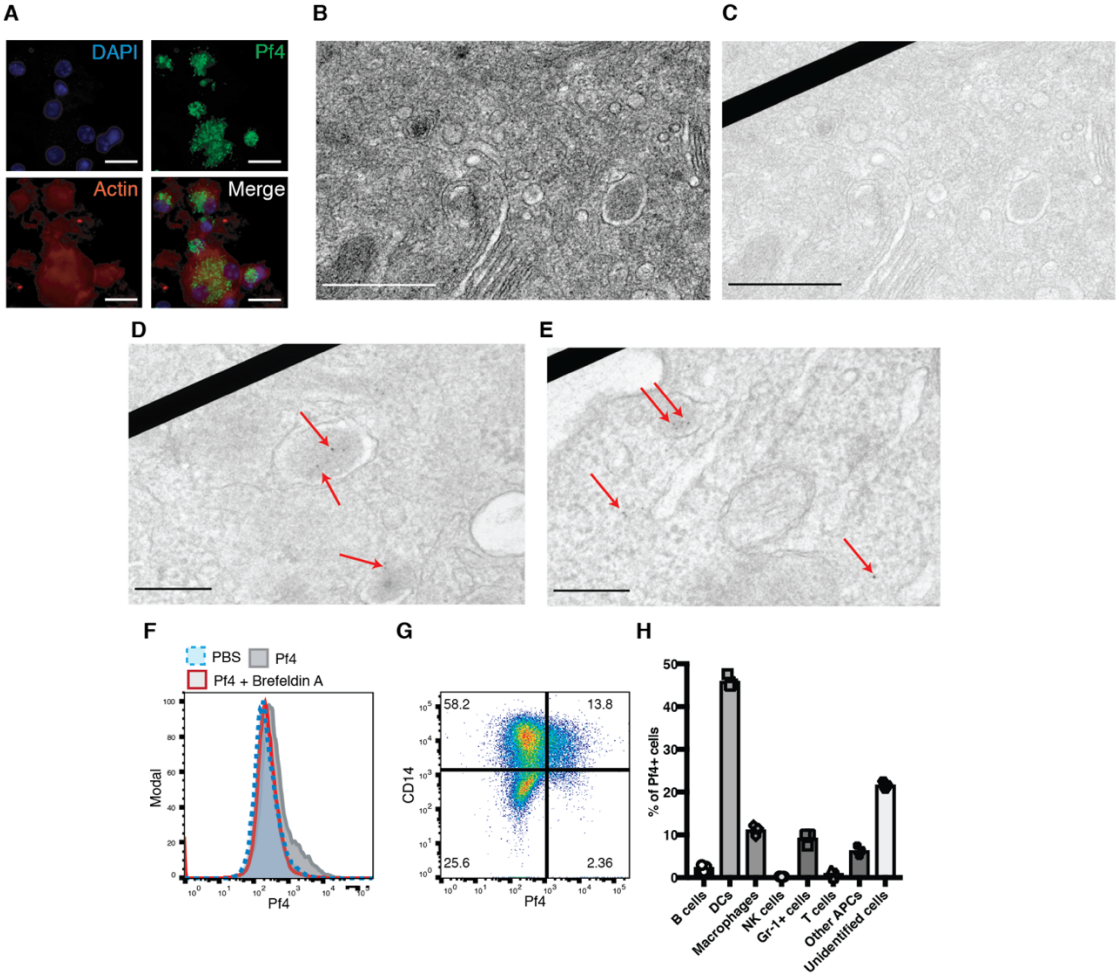

Figure S11. Pf4 phage are internalized by BMDCs. A) Immunofluorescence microscopy of Pf4 uptake by murine BMDCS stimulated with fluorescently labeled Pf4. Scale bar: 25 μm. B) TEM image of BMDCs without Pf4 stimulation (negative control to Fig. 5D-E). Magnification 15,000×. C) Same image as (B) but with beam blocker to enhance gold contrast. Scale bars in (B-C): 500 nm. D) Beam blocker image of Fig. 5D. E) Beam blocker image of Fig. 5E. Scale bars in (D-E): 200 nm. F) Pf4 uptake by BMDCs treated with vesicular transport inhibitor brefeldin A. G) Flow cytometry analysis of Pf4 uptake by CD14-positive cells. H) Percentage of individual immune cell populations within wound-infiltrating immune cells that took up Pf4. (A, F-H) are representative of $n \geq 3$ experiments with $n \geq 3$ replicates.

Fig. S12

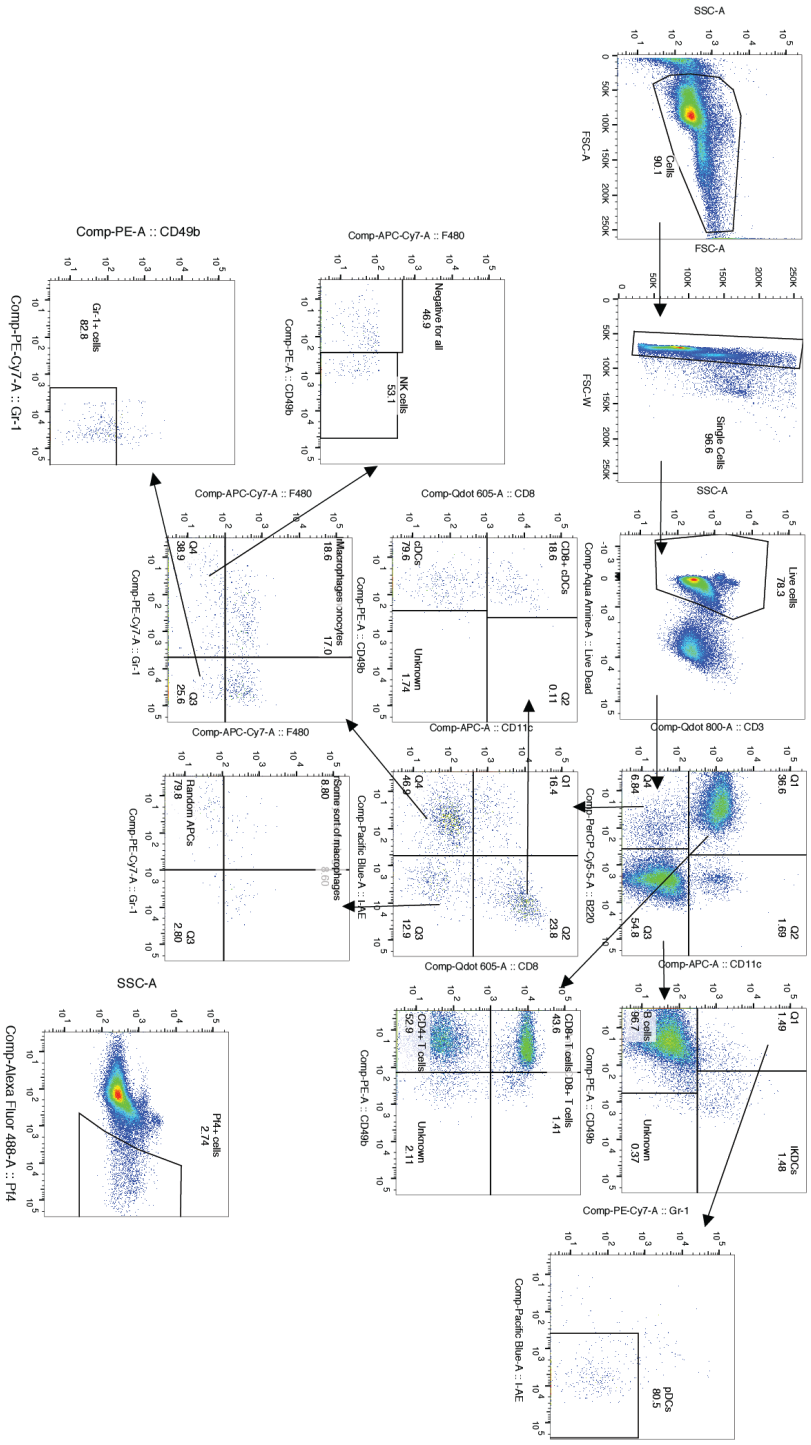

Figure S12. Representative gating schematic for the flow cytometric analysis of spleen and lymph node cells in Fig. 5G-H.

Fig. S13

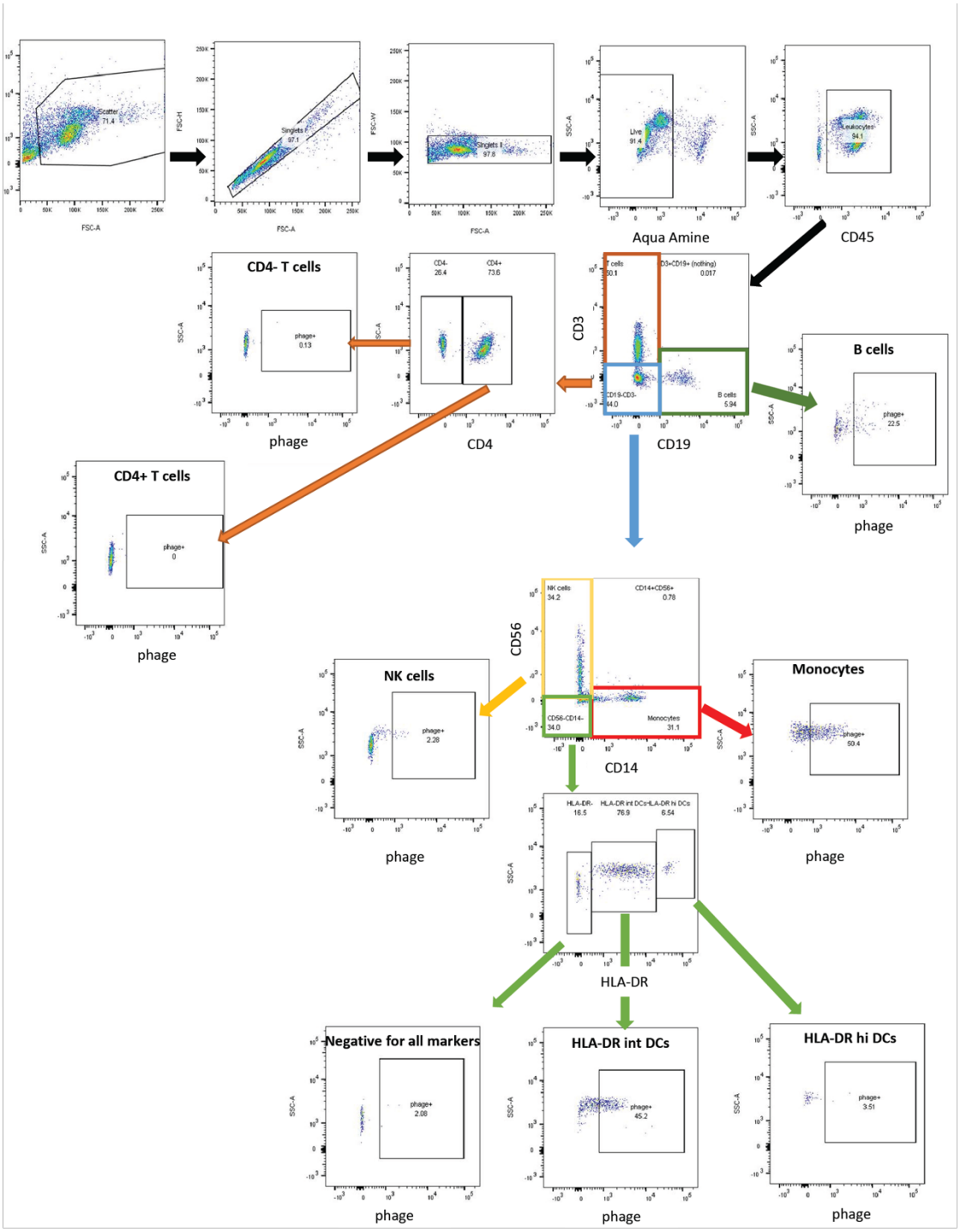

Figure S13. Representative gating schematic for the flow cytometric analysis of human PBMCs in Fig. 5I-J.

Fig. S14

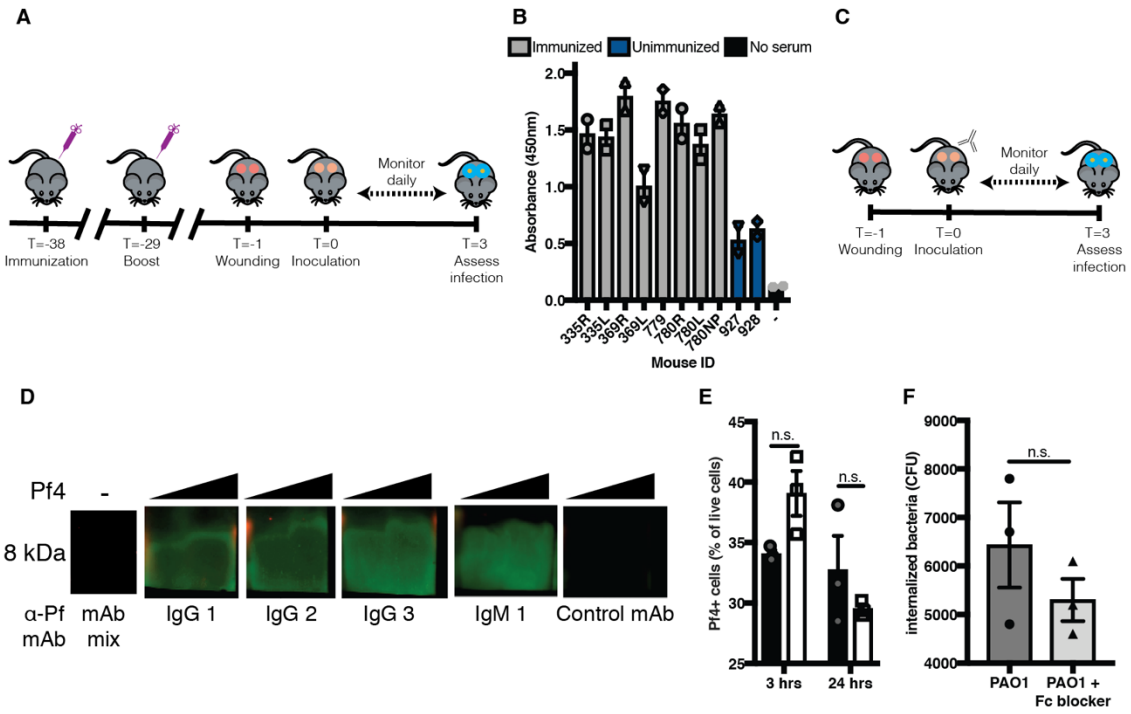

Figure S14. Vaccination against Pf phage peptide raises protective antibodies that do not impact Pf phage internalization. A) Vaccination protocol for immunization with KLH-conjugated CoaB peptide. B) Absorbance signal from Pf phage-specific antibody ELISA using serum from mice immunized with CoaB peptide. C) Passive immunization protocol with monoclonal antibodies against CoaB. D) Immunoblot with denatured Pf phage probed with various monoclonal antibodies against phage CoaB coat protein (molecular weight CoaB=8.4 kDa) or a control mAb. E) Pf phage uptake by BMDCs treated with anti-Pf mAbs for 3 hours or 24 hours. F) Phagocytosis of PAO1 by BMDCs treated with Fc blocker. (E-F) are representative of n=3 experiments with n=3 replicates. Depicted are mean and SEM. Statistics: two-tailed Student's t-test.

Table S1

	Pa(+)Pf(-)	*Pa*(+)Pf(+)	p-value
Total (*n*, %)	12, 32%	25, 68%	-
Age of patient in years - Mean (SD)	75.08 (4.3)	61.6 (2.9)	0.0131
Gender (*n*) - Male - Female	6 (50%) 6 (50%)	9 (36%) 16 (64%)	0.4879
Race / ethnicity - Caucasian - Asian - Hispanic - African-American	6 (50%) 1 (8%) 5 (42%) 0 (0%)	17 (68%) 3 (12%) 3 (12%) 2 (8%)	0.1883
Body mass index in kg/m^2 - Mean (SD)	29.63 (2.0)	27.95 (2.4)	0.6546
Age of wound in years - Median - Range	0.5 0.1-10.5	2.1 0.35-20.5	0.0252
Comorbidities - Diabetes Mellitus - Renal disease	4 (33%) 1 (8%)	12 (48%) 8 (32%)	0.4912 0.2204
Recurrence of infection	3 (43%)	9 (43%)	
Coinfection - *Staphylococcus aureus* - Other Gram-positive - Other Gram-negatives - *Candida* species	8 (67%) 4 (33%) 3 (25%) 5 (42%) 1 (8%)	19 (76%) 10 (40%) 8 (32%) 11 (44%) 0 (0%)	0.6964 >0.999 >0.999 >0.999 0.3243

Table S1. Patient database for human wound infection swab collection. Clinical information on the patients with culture-positive *Pseudomonas aeruginosa* (*Pa*) infected non-healing wounds who participated in the wound swab study. Renal Disease was defined as patients with Chronic Kidney Disease or End Stage Renal Disease. Statistical significance was measured using Fisher's exact test for the following parameters: Gender, Infection Recurrence, Diabetes status, and Renal Disease status. Statistical significance was measured using an unpaired Student's *t*-test for Patient age and BMI, a chi-squared test for Race/Ethnicity, and an unpaired two-tailed Mann-Whitney test for Wound Age. Nine patients were excluded from the Infection Recurrence analysis because they did not provide an answer on the patient questionnaire. SD = standard deviation.

Table S2

Name	Sequence (5'→3')	Fragment length (bp)	Gene length (bp)
T7_PAO723_F	**TAATACGACTCACTATAG**AGCAATGAAGCAACGCATCG	238	248
T7_PAO723_R	CTTGCGCAACATGCTGTAGA		
T7_PAO724_F	**TAATACGACTCACTATAG**CGATGAAGTTTGCGAGCCTG	1279	1262
T7_PAO724_R	CGAGAAAACCGGAGAGCCAT		
T7_PAO727_F	**TAATACGACTCACTATAG**AGCCACCTATTGCGGTTTCA	1428	1292
T7_PAO727_R	CTTGGTCTTGAACCGCTTGC		
T7_PAO728_F	**TAATACGACTCACTATAG**GACTCGTCGCGATCTGGAAA	1064	983
T7_PAO728_R	AGCCTTCAACCTATGAGCGG		
PAO717_F	TTCCCGCGTGGAATGC		
PAO717_R	CGGGAAGACAGCCACCAA		
PAO717_probe	AACGCTGGGTCGAAG		
Pf4_ig_F	GGAAGCAGCGCGATGAA		
Pf4_ig_R	GGAGCCAATCGCAAGCAA		
Pf4_ig_probe	CAATTGCGCTGGTGAA		
PAO724_5F	ACCTGGGAAAAGAAGGTCGAG		
PAO724_5R	GATCGACGTTGGCCTTCACC		
PAO727_5F	CGGTCTACGATCCGTTCTGG		
PAO727_5R	GATCGCACTCGACCTGGAC		
PAO728_1F	GTCTCTCGGAGTTGGTCGAA		
PAO728_1R	AACGATGCCCGTTGCTCAAG		
Pf_int_2F	CAATGGTCGTCACGCAGAAC		
Pf_int_2R	CACCAGCGCAATTGCTTCAT		
PAO728_1R	AACGATGCCCGTTGCTCAAG		
Pf_int_2F	CAATGGTCGTCACGCAGAAC		
Pf_int_2R	CACCAGCGCAATTGCTTCAT		
*Tnf*_F	CAGGCGGTGCCTATGTCTC		
*Tnf*_R	CGATCACCCCGAAGTTCAGTAG		
*Actb*_F	GGCTGTATTCCCCTCCATCG		
*Actb*_R	CCAGTTGGTAACAATGCCATGT		
rplU_F	CAAGGTCCGCATCATCAAGTT		
rplU_R	GGCCCTGACGCTTCATGT		
rplU_probe	CGCCGTCGTAAGC		

Table S2. Primers and probes used in this study.

Table S3

Target	Clone	Application	Manufacturer	Conjugate	Concentration Used	Host Species	Species Targeted
B220	RA3-6B2	Flow Cytometry	BioLegend, Cat. No. 103236	PerCP/Cy5.5	5 µg/mL	Rat	Mouse
I-A/I-E	M5/114.15.2	Flow Cytometry	BioLegend, Cat. No. 107620	Pacific Blue	5 µg/mL	Rat	Mouse
CD11c	N418	Flow Cytometry	BioLegend, Cat. No. 117310	APC	1 µg/mL	Armenian Hamster	Mouse
F4/80	BM8	Flow Cytometry	BioLegend Cat. No. 123118	APC/Cy7	1 µg/mL	Rat	Mouse
CD49b	DX5	Flow Cytometry	Invitrogen, Cat. No. 12-5971-82	PE	1 µg/mL	Rat	Mouse
CD11b	M1/70	Flow Cytometry	Invitrogen, Cat. No. 53-0112-80	Alexa Fluor 488	1 µg/mL	Rat	Mouse
Gr-1	RB6-8C5	Flow Cytometry	BioLegend, Cat. No. 108416	PE/Cy7	1 µg/mL	Rat	Mouse
CD3	17A2	Flow Cytometry	BioLegend, Cat. No. 100232	Brilliant Violet 785	5 µg/mL	Rat	Mouse
CD8	53-6.7	Flow Cytometry	BioLegend, Cat. No. 100744	Brilliant Violet 605	5 µg/mL	Rat	Mouse
CD14	Sa14-2	Flow Cytometry	BioLegend, Cat. No. 123314	PerCP/Cy5.5	1 µg/mL	Rat	Mouse
CD64	X54-5/7.1	Flow Cytometry	BioLegend, Cat. No. 139307	PerCP/Cy5.5	1 µg/mL	Mouse	Mouse
TNF	Mab22	Flow Cytometry	BioLegend, Cat. No. 502909	PE	1 µg/mL	Mouse	Mouse
TNF	1F3F3D4	ELISA	Invitrogen, Cat. 14-7325-85		2.5 µg/mL	Rat	Mouse
TNF	MP6-XT22/ MP6-XT3	ELISA	Invitrogen, Cat. No. 13-7326-85	Biotin	1.25 µg/mL	Rat	Mouse
CD3	UCHT1	Flow Cytometry	Biosciences, Cat. No. 557943	Alexa Fluor 700	2 µg/mL	Mouse	Human
CD4	RPA-T4	Flow Cytometry	BioLegend, Cat. No. 300511	PE/Cy7	1 µg/mL	Mouse	Human
CD14	63D3	Flow Cytometry	BioLegend, Cat. No. 367109	PerCP/Cy5.5	2 µg/mL	Mouse	Human
CD19	HIB19	Flow Cytometry	BioLegend, Cat. No. 302211	APC	2 µg/mL	Mouse	Human
CD45	HI30	Flow Cytometry	BioLegend, Cat. No. 304014	APC/Cy7	2 µg/mL	Mouse	Human
HLA-DR	L243	Flow Cytometry	BioLegend, Cat. No. 307623	Pacific Blue	2 µg/mL	Mouse	Human
CD56	HCD56	Flow Cytometry	BioLegend, Cat. No. 318305	PE	2 µg/mL	Mouse	Human
TLR3	Ab62566	Microscopy	AbCam, Cat. No. ab62566		1 µg/mL	Rabbit	Mouse
NF-κB p65	C-20	Immuno-blotting	Santa Cruz Biotechnology, Cat. No. sc372		1 µg/mL	Rabbit	Mouse
HSP90	4874	Immuno-blotting	Cell Signaling Technology, Cat. No. 4874		1 µg/mL	Rabbit	Mouse
Lamin-B	C-20	Immuno-blotting	Santa Cruz Biotechnology, Cat. No. sc-6216		1 µg/mL	Goat	Mouse
IκBα	9242	Immuno-blotting	Cell Signaling Technology, Cat. No. 9242		1 µg/mL	Rabbit	Mouse
Goat IgG		Immuno-blotting	Jackson ImmunoResearch Laboratories, Cat. No. 205-032-176	HRP	1:25,000	Mouse	Goat

Rabbit IgG		Immuno-blotting	Jackson ImmunoResearch Laboratories, Cat. No. 211-032-171	HRP	1:25,000	Mouse	Rabbit

Table S3. Antibodies used in this study.

Movie S1

3D image of BMDC internalizing Pf4 phage after 3 hours of incubation. Purple = actin stain. Blue = DAPI stain. Green = Alexa Fluor 488-labeled Pf4.

References and Notes

1. E. A. Azzopardi, E. Azzopardi, L. Camilleri, J. Villapalos, D. E. Boyce, P. Dziewulski, W. A. Dickson, I. S. Whitaker, Gram negative wound infection in hospitalised adult burn patients—Systematic review and metanalysis-. *PLOS ONE* **9**, e95042 (2014). doi:10.1371/journal.pone.0095042 Medline

2. K. Kirketerp-Møller, P. O. Jensen, M. Fazli, K. G. Madsen, J. Pedersen, C. Moser, T. Tolker-Nielsen, N. Høiby, M. Givskov, T. Bjarnsholt, Distribution, organization, and ecology of bacteria in chronic wounds. *J. Clin. Microbiol.* **46**, 2717–2722 (2008). doi:10.1128/JCM.00501-08 Medline

3. C. K. Sen, G. M. Gordillo, S. Roy, R. Kirsner, L. Lambert, T. K. Hunt, F. Gottrup, G. C. Gurtner, M. T. Longaker, Human skin wounds: A major and snowballing threat to public health and the economy. *Wound Repair Regen.* **17**, 763–771 (2009). doi:10.1111/j.1524-475X.2009.00543.x Medline

4. S. Shrivastava, P. Shrivastava, J. Ramasamy, World Health Organization releases global priority list of antibiotic-resistant bacteria to guide research, discovery, and development of new antibiotics. *J. Med. Soc.* **32**, 76–77 (2018). doi:10.4103/jms.jms_25_17

5. T.-B. Tsay, M.-C. Yang, P.-H. Chen, K.-H. Lai, H.-T. Huang, C.-M. Hsu, L.-W. Chen, Blocking TNF-α enhances Pseudomonas aeruginosa-induced mortality in burn mice through induction of IL-1β. *Cytokine* **63**, 58–66 (2013). doi:10.1016/j.cyto.2013.04.002 Medline

6. D. Gosselin, J. DeSanctis, M. Boulé, E. Skamene, C. Matouk, D. Radzioch, Role of tumor necrosis factor alpha in innate resistance to mouse pulmonary infection with Pseudomonas aeruginosa. *Infect. Immun.* **63**, 3272–3278 (1995). Medline

7. R. T. Sadikot, H. Zeng, M. Joo, M. B. Everhart, T. P. Sherrill, B. Li, D. S. Cheng, F. E. Yull, J. W. Christman, T. S. Blackwell, Targeted immunomodulation of the NF-κB pathway in airway epithelium impacts host defense against Pseudomonas aeruginosa. *J. Immunol.* **176**, 4923–4930 (2006). doi:10.4049/jimmunol.176.8.4923 Medline

8. S. L. Gellatly, R. E. W. Hancock, Pseudomonas aeruginosa: New insights into pathogenesis and host defenses. *Pathog. Dis.* **67**, 159–173 (2013). doi:10.1111/2049-632X.12033 Medline

9. M. Alhede, T. Bjarnsholt, M. Givskov, M. Alhede, *Pseudomonas aeruginosa Biofilms: Mechanisms of Immune Evasion* (Elsevier, ed. 1, 2014), vol. 86.

10. J. S. Webb, M. Lau, S. Kjelleberg, Bacteriophage and phenotypic variation in Pseudomonas aeruginosa biofilm development. *J. Bacteriol.* **186**, 8066–8073 (2004). doi:10.1128/JB.186.23.8066-8073.2004 Medline

11. S. A. Rice, C. H. Tan, P. J. Mikkelsen, V. Kung, J. Woo, M. Tay, A. Hauser, D. McDougald, J. S. Webb, S. Kjelleberg, The biofilm life cycle and virulence of Pseudomonas aeruginosa are dependent on a filamentous prophage. *ISME J.* **3**, 271–282 (2009). doi:10.1038/ismej.2008.109 Medline

12. P. R. Secor, J. M. Sweere, L. A. Michaels, A. V. Malkovskiy, D. Lazzareschi, E. Katznelson, J. Rajadas, M. E. Birnbaum, A. Arrigoni, K. R. Braun, S. P. Evanko, D. A. Stevens, W. Kaminsky, P. K. Singh, W. C. Parks, P. L. Bollyky, Filamentous Bacteriophage Promote Biofilm Assembly and Function. *Cell Host Microbe* **18**, 549–559 (2015). doi:10.1016/j.chom.2015.10.013 Medline

13. P. R. Secor, L. A. Michaels, K. S. Smigiel, M. G. Rohani, L. K. Jennings, K. B. Hisert, A. Arrigoni, K. R. Braun, T. P. Birkland, Y. Lai, T. S. Hallstrand, P. L. Bollyky, P. K. Singh, W. C. Parks, Filamentous Bacteriophage Produced by *Pseudomonas aeruginosa* Alters the Inflammatory Response and Promotes Noninvasive Infection In Vivo. *Infect. Immun.* **85**, e00648-16 (2016). doi:10.1128/IAI.00648-16 Medline

14. A. Mai-Prochnow, J. G. K. Hui, S. Kjelleberg, J. Rakonjac, D. McDougald, S. A. Rice, 'Big things in small packages: The genetics of filamentous phage and effects on fitness of their host'. *FEMS Microbiol. Rev.* **39**, 465–487 (2015). doi:10.1093/femsre/fuu007 Medline

15. E. Martínez, J. Campos-Gómez, Pf Filamentous Phage Requires UvrD for Replication in Pseudomonas aeruginosa. *MSphere* **1**, e00104 (2016). Medline

16. P. Knezevic, M. Voet, R. Lavigne, Prevalence of Pf1-like (pro)phage genetic elements among Pseudomonas aeruginosa isolates. *Virology* **483**, 64–71 (2015). doi:10.1016/j.virol.2015.04.008 Medline

17. G. Chaby, V. Viseux, A. A. Ramelet, O. Ganry, A. Billet, C. Lok, Refractory venous leg ulcers: A study of risk factors. *Dermatol. Surg.* **32**, 512–519 (2006). Medline

18. P. J. Franks, C. J. Moffatt, M. Connolly, N. Bosanquet, M. I. Oldroyd, R. M. Greenhalgh, C. N. McCollum, Factors associated with healing leg ulceration with high compression. *Age Ageing* **24**, 407–410 (1995). doi:10.1093/ageing/24.5.407 Medline

19. C. J. Moffatt, P. J. Franks, M. Oldroyd, N. Bosanquet, P. Brown, R. M. Greenhalgh, C. N. McCollum, Community clinics for leg ulcers and impact on healing. *BMJ* **305**, 1389–1392 (1992). doi:10.1136/bmj.305.6866.1389 Medline

20. J. S. Chen, M. T. Longaker, G. C. Gurtner, in *Methods in Molecular Biology* (Humana Press, Totowa, NJ, 2013), vol. 1037 of *Methods in Molecular Biology*, pp. 265–274.

21. J. Park, J. E. Babensee, Differential functional effects of biomaterials on dendritic cell maturation. *Acta Biomater.* **8**, 3606–3617 (2012). doi:10.1016/j.actbio.2012.06.006 Medline

22. D. Yang, K. S. Jones, Effect of alginate on innate immune activation of macrophages. *J. Biomed. Mater. Res. A* **90**, 411–418 (2009). doi:10.1002/jbm.a.32096 Medline

23. T. Cantaert, D. Baeten, P. P. Tak, L. G. M. van Baarsen, Type I IFN and TNFα cross-regulation in immune-mediated inflammatory disease: Basic concepts and clinical relevance. *Arthritis Res. Ther.* **12**, 219 (2010). doi:10.1186/ar3150 Medline

24. I. Sauer, B. Schaljo, C. Vogl, I. Gattermeier, T. Kolbe, M. Müller, P. J. Blackshear, P. Kovarik, Interferons limit inflammatory responses by induction of tristetraprolin. *Blood* **107**, 4790–4797 (2006). doi:10.1182/blood-2005-07-3058 Medline

25. T. Kawasaki, T. Kawai, Toll-like receptor signaling pathways. *Front. Immunol.* **5**, 461 (2014). doi:10.3389/fimmu.2014.00461 Medline

26. A.-J. Tong, X. Liu, B. J. Thomas, M. M. Lissner, M. R. Baker, M. D. Senagolage, A. L. Allred, G. D. Barish, S. T. Smale, A Stringent Systems Approach Uncovers Gene-Specific Mechanisms Regulating Inflammation. *Cell* **165**, 165–179 (2016). doi:10.1016/j.cell.2016.01.020 Medline

27. L. Wang, E. Trebicka, Y. Fu, L. Waggoner, S. Akira, K. A. Fitzgerald, J. C. Kagan, B. J. Cherayil, Regulation of lipopolysaccharide-induced translation of tumor necrosis factor-alpha by the toll-like receptor 4 adaptor protein TRAM. *J. Innate Immun.* **3**, 437–446 (2011). doi:10.1159/000324833 Medline

28. T. Abe, A. Harashima, T. Xia, H. Konno, K. Konno, A. Morales, J. Ahn, D. Gutman, G. N. Barber, STING recognition of cytoplasmic DNA instigates cellular defense. *Mol. Cell* **50**, 5–15 (2013). doi:10.1016/j.molcel.2013.01.039 Medline

29. D. Gao, T. Li, X.-D. Li, X. Chen, Q.-Z. Li, M. Wight-Carter, Z. J. Chen, Activation of cyclic GMP-AMP synthase by self-DNA causes autoimmune diseases. *Proc. Natl. Acad. Sci. U.S.A.* **112**, E5699–E5705 (2015). doi:10.1073/pnas.1516465112 Medline

30. A. Baird, Gene transfer into Mammalian cells using targeted filamentous bacteriophage. *Cold Spring Harb. Protoc.* **2011**, 950–957 (2011). doi:10.1101/pdb.prot5653 Medline

31. S. N. Lester, K. Li, Toll-like receptors in antiviral innate immunity. *J. Mol. Biol.* **426**, 1246–1264 (2014). doi:10.1016/j.jmb.2013.11.024 Medline

32. Z. Kaźmierczak, A. Piotrowicz, B. Owczarek, K. Hodyra, P. Miernikiewicz, D. Lecion, M. Harhala, A. Górski, K. Dąbrowska, Molecular imaging of T4 phage in mammalian tissues and cells. *Bacteriophage* **4**, e28364–e28366 (2014). doi:10.4161/bact.28364 Medline

33. M. Gaubin, C. Fanutti, Z. Mishal, A. Durrbach, P. De Berardinis, R. Sartorius, G. Del Pozzo, J. Guardiola, R. N. Perham, D. Piatier-Tonneau, Processing of filamentous bacteriophage virions in antigen-presenting cells targets both HLA class I and class II peptide loading compartments. *DNA Cell Biol.* **22**, 11–18 (2003). doi:10.1089/104454903321112451 Medline

34. Y. Tian, M. Wu, X. Liu, Z. Liu, Q. Zhou, Z. Niu, Y. Huang, Probing the endocytic pathways of the filamentous bacteriophage in live cells using ratiometric pH fluorescent indicator. *Adv. Healthc. Mater.* **4**, 413–419 (2015). doi:10.1002/adhm.201400508 Medline

35. H.-K. Lee, S. Dunzendorfer, K. Soldau, P. S. Tobias, Double-stranded RNA-mediated TLR3 activation is enhanced by CD14. *Immunity* **24**, 153–163 (2006). doi:10.1016/j.immuni.2005.12.012 Medline

36. S. Nguyen, K. Baker, B. S. Padman, R. Patwa, R. A. Dunstan, T. A. Weston, K. Schlosser, B. Bailey, T. Lithgow, M. Lazarou, A. Luque, F. Rohwer, R. S. Blumberg, J. J. Barr, Bacteriophage Transcytosis Provides a Mechanism To Cross Epithelial Cell Layers. *mBio* **8**, e01874 (2017). doi:10.1128/mBio.01874-17 Medline

37. K. Hodyra-Stefaniak, P. Miernikiewicz, J. Drapała, M. Drab, E. Jończyk-Matysiak, D. Lecion, Z. Kaźmierczak, W. Beta, J. Majewska, M. Harhala, B. Bubak, A. Kłopot, A. Górski, K. Dąbrowska, Mammalian Host-Versus-Phage immune response determines phage fate in vivo. *Sci. Rep.* **5**, 14802 (2015). Medline

38. E. Bille, J. Meyer, A. Jamet, D. Euphrasie, J.-P. Barnier, T. Brissac, A. Larsen, P. Pelissier, X. Nassif, A virulence-associated filamentous bacteriophage of Neisseria meningitidis increases host-cell colonisation. *PLOS Pathog.* **13**, e1006495 (2017). doi:10.1371/journal.ppat.1006495 Medline

39. E. Jończyk-Matysiak, M. Łusiak-Szelachowska, M. Kłak, B. Bubak, R. Międzybrodzki, B. Weber-Dąbrowska, M. Żaczek, W. Fortuna, P. Rogóż, S. Letkiewicz, K. Szufnarowski, A. Górski, The Effect of Bacteriophage Preparations on Intracellular Killing of Bacteria by Phagocytes. *J. Immunol. Res.* **2015**, 482863 (2015). doi:10.1155/2015/482863 Medline

40. J. D. Van Belleghem, F. Clement, M. Merabishvili, R. Lavigne, M. Vaneechoutte, Pro- and anti-inflammatory responses of peripheral blood mononuclear cells induced by *Staphylococcus aureus* and *Pseudomonas aeruginosa* phages. *Sci. Rep.* **7**, 8004 (2017). Medline

41. D. R. Roach, C. Y. Leung, M. Henry, E. Morello, D. Singh, J. P. Di Santo, J. S. Weitz, L. Debarbieux, Synergy between the Host Immune System and Bacteriophage Is Essential for Successful Phage Therapy against an Acute Respiratory Pathogen. *Cell Host Microbe* **22**, 38–47.e4 (2017). doi:10.1016/j.chom.2017.06.018 Medline

42. J. De Smet, H. Hendrix, B. G. Blasdel, K. Danis-Wlodarczyk, R. Lavigne, Pseudomonas predators: Understanding and exploiting phage-host interactions. *Nat. Rev. Microbiol.* **15**, 517–530 (2017). doi:10.1038/nrmicro.2017.61 Medline

43. S. M. Burns-Guydish, I. N. Olomu, H. Zhao, R. J. Wong, D. K. Stevenson, C. H. Contag, Monitoring age-related susceptibility of young mice to oral Salmonella enterica serovar Typhimurium infection using an in vivo murine model. *Pediatr. Res.* **58**, 153–158 (2005). doi:10.1203/01.PDR.0000157725.44213.C4 Medline

44. J. Sambrook, E. F. Fritsch, T. Maniatis, *Molecular Cloning. A Laboratory Manual* (Cold Spring Harbor Laboratory Press, Cold Spring Harbor, NY, ed. 1, 1989).

45. P. Boulanger, Purification of bacteriophages and SDS-PAGE analysis of phage structural proteins from ghost particles. *Methods Mol. Biol.* **502**, 227–238 (2009). doi:10.1007/978-1-60327-565-1_13 Medline

46. K. Zimmermann, H. Hagedorn, C. C. Heuck, M. Hinrichsen, H. Ludwig, The ionic properties of the filamentous bacteriophages Pf1 and fd. *J. Biol. Chem.* **261**, 1653–1655 (1986). Medline

47. H. Cho, S. Balaji, A. Q. Sheikh, J. R. Hurley, Y. F. Tian, J. H. Collier, T. M. Crombleholme, D. A. Narmoneva, Regulation of endothelial cell activation and angiogenesis by injectable peptide nanofibers. *Acta Biomater.* **8**, 154–164 (2012). doi:10.1016/j.actbio.2011.08.029 Medline

48. S. G. Keswani, S. Balaji, A. B. Katz, A. King, K. Omar, M. Habli, C. Klanke, T. M. Crombleholme, Intraplacental gene therapy with Ad-IGF-1 corrects naturally occurring rabbit model of intrauterine growth restriction. *Hum. Gene Ther.* **26**, 172–182 (2015). doi:10.1089/hum.2014.065 Medline

49. H. F. Kuipers, M. Rieck, I. Gurevich, N. Nagy, M. J. Butte, R. S. Negrin, T. N. Wight, L. Steinman, P. L. Bollyky, Hyaluronan synthesis is necessary for autoreactive T-cell trafficking, activation, and Th1 polarization. *Proc. Natl. Acad. Sci. U.S.A.* **113**, 1339–1344 (2016). doi:10.1073/pnas.1525086113 Medline

50. E. Amiel, R. R. Lovewell, G. A. O'Toole, D. A. Hogan, B. Berwin, Pseudomonas aeruginosa evasion of phagocytosis is mediated by loss of swimming motility and is independent of flagellum expression. *Infect. Immun.* **78**, 2937–2945 (2010). doi:10.1128/IAI.00144-10 Medline

51. P. Chomczynski, N. Sacchi, The single-step method of RNA isolation by acid guanidinium thiocyanate-phenol-chloroform extraction: Twenty-something years on. *Nat. Protoc.* **1**, 581–585 (2006). doi:10.1038/nprot.2006.83 Medline

52. J. A. Gebe, K. Yadava, S. M. Ruppert, P. Marshall, P. Hill, B. A. Falk, J. M. Sweere, H. Han, G. Kaber, I. A. Harten, C. Medina, K. Mikecz, S. F. Ziegler, S. Balaji, S. G. Keswani, V. A. Perez, M. J. Butte, K. Nadeau, W. A. Altemeier, N. Fanger, P. L. Bollyky, Modified High-Molecular-Weight Hyaluronan Promotes Allergen-Specific Immune Tolerance. *Am. J. Respir. Cell Mol. Biol.* **56**, 109–120 (2017). doi:10.1165/rcmb.2016-0111OC Medline

53. T. Horng, G. M. Barton, R. Medzhitov, TIRAP: An adapter molecule in the Toll signaling pathway. *Nat. Immunol.* **2**, 835–841 (2001). doi:10.1038/ni0901-835 Medline

54. Z. Jiang, P. Georgel, X. Du, L. Shamel, S. Sovath, S. Mudd, M. Huber, C. Kalis, S. Keck, C. Galanos, M. Freudenberg, B. Beutler, CD14 is required for MyD88-independent LPS signaling. *Nat. Immunol.* **6**, 565–570 (2005). doi:10.1038/ni1207 Medline

55. F. M. Tomley, in *Basic DNA and RNA Protocols*, A. J. Harwood, Ed. (Humana Press, Totowa, NJ, 1996), *Basic DNA and RNA Protocols*, pp. 359–362.

Science

Bacteriophage trigger antiviral immunity and prevent clearance of bacterial infection

Johanna M. Sweere, Jonas D. Van Belleghem, Heather Ishak, Michelle S. Bach, Medeea Popescu, Vivekananda Sunkari, Gernot Kaber, Robert Manasherob, Gina A. Suh, Xiou Cao, Christiaan R. de Vries, Dung N. Lam, Payton L. Marshall, Maria Birukova, Ethan Katznelson, Daniel V. Lazzareschi, Swathi Balaji, Sundeep G. Keswani, Thomas R. Hawn, Patrick R. Secor and Paul L. Bollyky

Science **363** (6434), eaat9691.
DOI: 10.1126/science.aat9691

Phage subverts immune response

Pseudomonas aeruginosa (*Pa*) is a multidrug-resistant Gramnegative bacterium commonly found in health care settings. *Pa* infections frequently result in considerable morbidity and mortality. Sweere *et al.* found that a type of temperate filamentous bacteriophage that infects and integrates into *Pa* is associated with chronic human wound infections. Likewise, wounds in mice colonized with phage-infected *Pa* were more severe and longer-lasting than those colonized by *Pa* alone. Immune cell uptake of phage-infected *Pa* resulted in phage RNA production and inappropriate antiviral immune responses, impeding bacterial clearance. Both phage vaccination and transfer of antiphage antibodies were protective against *Pa* infection.

Science, this issue p. eaat9691